Global enhancement of cortical excitability following coactivation of large neuronal populations

Deng Zhang[a,b,c,1] , Xingjian Yan[a,b,c,1] , Liang She[a,2], Yunqing Wen[a,c], and Mu-ming Poo[a,b,c,3]

[a]Institute of Neuroscience, State Key Laboratory of Neuroscience, Key Laboratory of Primate Neurobiology, Chinese Academy of Sciences Center for Excellence in Brain Science and Intelligence Technology, Chinese Academy of Sciences, 200031 Shanghai, China; [b]University of Chinese Academy of Sciences, 100049 Beijing, China; and [c]Shanghai Center for Brain Science and Brain-Inspired Intelligence Technology, 201210 Shanghai, China

Correlated activation of cortical neurons often occurs in the brain and repetitive correlated neuronal firing could cause long-term modifications of synaptic efficacy and intrinsic excitability. We found that repetitive optogenetic activation of neuronal populations in the mouse cortex caused enhancement of optogenetically evoked firing of local coactivated neurons as well as distant cortical neurons in both ipsilateral and contralateral hemispheres. This global enhancement of evoked responses required coactivation of a sufficiently large population of neurons either within one cortical area or distributed in several areas. Enhancement of neuronal firing was saturable after repeated episodes of coactivation, diminished by inhibition of N-methyl-D-aspartic acid receptors, and accompanied by elevated excitatory postsynaptic potentials, all consistent with activity-induced synaptic potentiation. Chemogenetic inhibition of neuronal activity of the thalamus decreased the enhancement effect, suggesting thalamic involvement. Thus, correlated excitation of large neuronal populations leads to global enhancement of neuronal excitability.

activity-dependent plasticity | synaptic potentiation | global excitability | cortical wave | corticothalamocortical circuit

Activity-dependent structural and functional plasticity is a fundamental property of the brain. For example, repetitive whisker stimulation could induce persistent elevation of evoked neuronal responses in the mouse primary somatosensory cortex (1, 2). A repetitive unidirectional moving bar in the visual field of the *Xenopus* tadpole enhanced the visual tectal neurons' response to the moving bar in the conditioned direction (3). Repetitive pairing of visual stimuli at two orientations in a unidirectional sequence induced a shift in the orientation tuning in the cat primary visual cortex (4). Serial application of finger stimuli changed the neuronal response specificity and maps of hand surfaces in the somatosensory cortical field of the monkey (5). Repetitive high-frequency auditory stimulation induced a long-lasting increase in the amplitude of sound-evoked potentials in the auditory cortex of humans (6). All these studies showed that repetitive sensory experiences could trigger long-term adapted changes at different levels of the cortex, leading to changes in the animal's responses to future sensory inputs.

Within a particular cortical region, sensory stimuli could coactivate large groups of cortical neurons (7–9). In the primary visual cortex (V1) of the mouse, single-cell two-photon optogenetic stimulation could recruit more neurons after repetitively coactivating groups of neurons in a small V1 area (240 × 240 μm), and this effect persisted for days (10). After the repetitive triggering of spike trains in a group of neurons within a 150-mm² area in layer 2/3 of mouse somatosensory cortex (S1), glutamate uncaging on these neurons triggered higher neuronal responses that were long-lasting (11). These findings suggest that correlated neuronal activities in a local cortical area may enhance synaptic efficacy or intrinsic neuronal excitability, or both, leading to long-term modification of local circuit functions.

Over many cortical areas, oscillations at various frequencies accompanying cognitive processes could coordinate neuronal activity at multiple scales to influence brain functions (12). A recent study showed that the human brain exhibits theta and alpha oscillations that travel from posterior to anterior cortices during the performance of memory tasks (13). The traveling wave could trigger sequential activation of cortical neurons over tens of milliseconds, resulting in strengthening of long-range cortical connections and a gradual increase of reverberating activity (14). The generation of the traveling wave at the whole-brain level depends on the synchronous local activation of cortical neurons. This is supported by the finding that large whisker deflection could evoke neuronal excitation in the mouse somatosensory cortex that spreads over the entire barrel field, while a weak whisker deflection led to excitation confining within a single barrel column (15). Sustained optogenetic activation of cortical neurons was also found to reliably induce global cortical waves (16).

In the present study, optogenetic methods were used to directly activate large populations of cortical pyramidal neurons in mouse cortices in a spatiotemporally controlled manner. We examined in detail the cellular mechanism underlying the enhanced neuronal excitability following repetitive neuronal coactivation, and determined the conditions of coactivation that are required for local induction and long-range spread of enhanced

Significance

Propagating cortical waves that evoke correlated firing of large neuronal populations may cause long-term modification of neural circuits in the brain. Using optogenetic stimulation, we found that repetitive coactivation of large populations of mouse cortical neurons led to enhanced excitability of cortical neurons in both coactivated areas and distant areas that were not coactivated, including those in the contralateral cortices. This global enhancement of neuronal excitability caused by local neuronal stimulation was accompanied by the potentiation of excitatory synaptic transmission, suggesting activity-dependent synaptic plasticity. The corticothalamocortical circuit could contribute to the propagation of this enhancement effect. These results show that the repetitive correlated excitation of large neuronal populations could lead to global enhancement of neuronal excitability.

www.manaraa.com

neuronal excitability. We first show that repetitive optogenetic activation of a substantial number of neurons in mouse V1 indeed resulted in postactivation persistent enhancement of optogenetically evoked firing of cortical neurons. Subsequent experiments showed that coactivation of a sufficiently large neuronal population was required for the enhancement effect, regardless of whether the neurons were localized within one cortical area or distributed in different cortical areas within the ipsilateral hemisphere or in both hemispheres. In vivo whole-cell recording of synaptic responses showed that activity-induced, N-methyl-D-aspartic acid (NMDA) receptor-dependent long-term potentiation of cortical excitatory synapses contributed to the enhancement of neuronal responses. These results provide insights into the dynamics of long-range interactions among cortical neurons and the consequence of repetitive coactivation of large populations of cortical neurons.
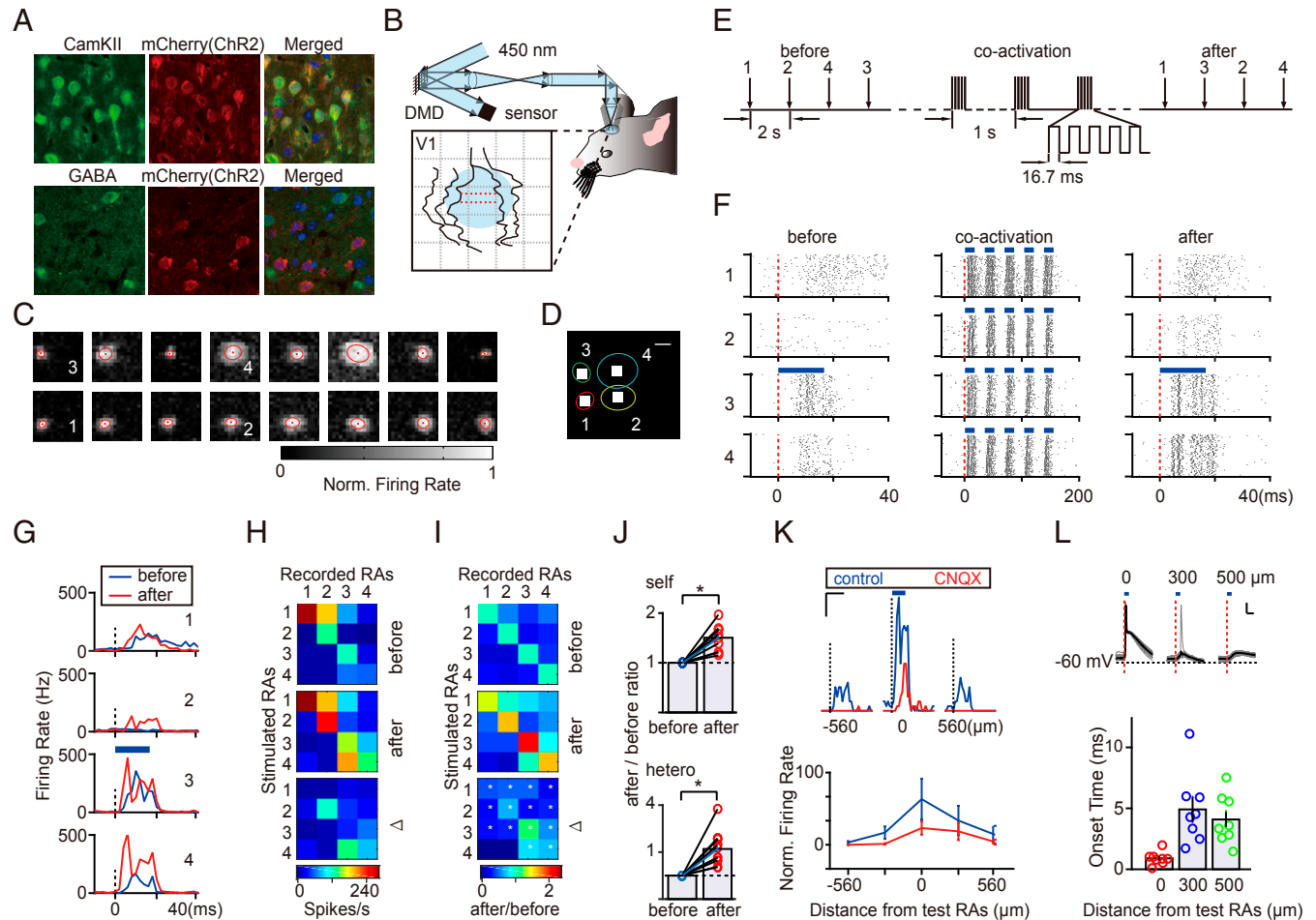

Fig. 1. Repetitive coactivation of cortical neurons enhances evoked spiking. (A) Images of a mouse V1 section, showing extensive colocalization of CaMKII immunostaining (green; *Top*) and poor colocalization of GABA immunostaining (green; *Bottom*) with ChR-2a-mCherry. (B) The experimental setup, showing a multielectrode array (red dots) inserted in V1 of the right hemisphere and a DMD for projecting blue light to V1. (C) Multiunit response areas in V1, recorded simultaneously by 16 electrodes in anesthetized mice. Ellipses, Gaussian fit at 1 SD. 1 to 4 indicate four spatially separated response areas monitored by four electrodes. (D) Four example RAs in C. White spots, optogenetic stimulation sites. (Scale bar, 200 μm.) (E) Experimental protocol. Test stimuli (before and after, four each shown), light pulse duration 16.7 ms, 50 pulses at 2-s intervals, applied in random sequence to four RAs. Coactivation, 50 bursts at 1-s intervals, five pulses per burst at 30 Hz. (F) Data from the example experiment. Peristimulus raster plots of spike trains in four RAs, in response to test stimuli applied to RA3, before, during, and after coactivation, over 50 trials. Red dashed line, light stimulus onset. Blue bar, light stimulation (16.7 ms). (G) Data from F shown in peristimulus histograms, for spike trains at all four RAs evoked by RA3 test stimulation, before (blue line) and after (red line) coactivation. Dark dashed line, onset of the stimulus. Blue bar, light stimulation. (H and I) Summary of changes (H, for the above example experiment; I, for all mice; n = 12) in spiking responses evoked by test stimuli applied sequentially to all four RAs, shown by heatmaps. In H, colors encode the evoked spiking (averaged firing rate over the first 30 ms after stimulus onset), before and after the coactivation, and the difference of spiking responses (Δ = after − before, positive for all). In I, colors encode the ratio of evoked spiking relative to self-activated spiking (diagonal values) before coactivation for each mouse. Positive differences of spiking response ratios (Δ = after − before) are marked by an asterisk. (J) Pairwise comparison of the after/before ratio of evoked spiking response at all RAs (defined as in H) for stimulus applied on itself (self) and to other RAs (hetero) before (blue) and after coactivation. Each data point represents the average ratio for all tested RAs observed in one mouse (*P < 0.01 for both datasets, paired t test; n = 12 mice). (K) The effect of CNQX on stimulus-evoked responses. (K, Top) Evoked spiking responses before (blue line) and after (red line) CNQX infusion (0.5 mM) in hetero RAs (lateral, 560 μm) and self-activated RA (*Middle*; 0 μm). (Scale bars, 20 ms, 100 Hz.) Blue bar, test laser stimulus. (K, Bottom) Summary of all experiments (n = 5 mice), showing 50% reduction and complete elimination of self-activated and hetero responses, respectively. (L) EPSPs evoked by test stimuli applied at three different distances (0, 300, and 500 μm) from the whole-cell recorded neurons in one example experiment (*Top*), for single trials (gray lines), and averaged over 50 trials (black lines). Blue bar, test light stimulus (duration 16.7 ms). Histograms (*Bottom*) depict the average onset time of test-evoked EPSPs at three different distances from the test stimulation site, recorded from eight neurons from six mice. The differences between the data at 0 μm and those at 300 and 500 μm were significant (P < 0.001, one-way ANOVA, followed by Bonferroni post hoc test). (Scale bars, 25 ms, 10 mV.)

Zhang et al.

www.manaraa.com

Results

Repetitive Coactivation of Cortical Neurons Enhances Evoked Spiking.

For optogenetic stimulation of large populations of cortical neurons, we injected adult mouse V1 with an adeno-associated virus (AAV) vector that expressed channelrhodopsin-2 (ChR2)-2a-mCherry under the promoter for calmodulin-dependent protein kinase II α (CaMKIIα). The selectivity of mCherry expression in cortical neurons was confirmed by immunostaining of cortical slices of AAV-injected mice. Among all mCherry+ neurons, $84 \pm 3\%$ showed CaMKIIα immunostaining ($n = 252$ cells, 3 mice, 8 slices), and only $10 \pm 11\%$ showed immunostaining of γ-aminobutyric acid (GABA) ($n = 246$ cells, 4 mice, 8 slices). Thus, ChR2 expression was largely selective for excitatory V1 neurons (Fig. 1*A*).

Cortical neuronal activities were monitored by two linear arrays of multiunit electrodes (eight units each). The electrodes were inserted into L2/3 of mouse V1 at a depth of ~300 μm (Fig. 1*B*). A laser-stimulation system based on a digital microarray device (DMD; resolution 608×684) was used to stimulate ChR2-expressing neuronal groups with specific spatiotemporal patterns. We first mapped the area of optogenetic stimulation that evoked multiunit responses at each electrode (termed hereafter "response area"; RA) using blue-light spots (duration ~80 ms, ~130×130 μm, 4 mW/mm²) that were delivered with a sparse-noise pattern to V1 of anesthetized mice. As illustrated in Fig. 1*C*, RAs were found to be topographically associated with the array electrodes. In the example experiment described below (Fig. 1*D*), we chose four well-separated RAs (at the corners of a rectangle), with average distances of 378 ± 18 μm between the centers of adjacent RAs. To estimate the relationship between the light intensity and evoked response in RAs, we randomly activated each RA and monitored multiunit spiking responses in all RAs. When the intensity of the test light at one RA was increased, the total number of evoked spikes increased and the onset of spiking decreased at all four RAs (*SI Appendix*, Fig. S1). The procedures for estimating the intensity of the test and coactivation stimuli are described in *Materials and Methods*. We chose the intensity at which the test stimulation at the center of an RA evoked multiunit firing at all four electrodes, as indicated by the peristimulus time histogram (PSTH) in *SI Appendix*, Fig. S1 *A*, *Bottom*.

In the first set of experiments, we examined whether repetitive synchronous coactivation of multiple neuronal populations in all four RAs in V1 of anesthetized mice could alter the rate of multiunit spiking evoked by the "test" stimuli. Spiking recorded at all four electrodes was monitored when test stimuli were applied individually to each RA before and after coactivation. The test stimuli were applied to the center of each RA in a random sequence at a low frequency (0.08 to 0.5 Hz, with random intervals in the range of 2 to 12 s, pulse duration 16.7 ms). The coactivation protocol consisted of repetitive synchronous application of stimuli (with the same size and intensity as the test stimulus) at a higher frequency (50 bursts at 1-s intervals, 5 pulses per burst at 30 Hz; *Materials and Methods*) at the selected RAs (Fig. 1*E*).

As shown in Fig. 1 *F* and *G*, we recorded multiunit spiking at each of the four electrodes in response to the test stimuli applied at "RA3" (50 trials), before and after coactivation of all four RAs. The spiking rasters showed that RA3-evoked responses at all four RAs were all elevated after coactivation (Fig. 1*F*). This effect was also depicted by the PSTH of spiking rates for all four RAs evoked by the test stimulation of RA3 (Fig. 1*G*).

The enhancement effect was also revealed by the matrix plot of normalized spike rates at each RA (total spike count over the 30-ms period after the test stimulus onset; color-coded) in response to the test stimulus at each of the four RAs, before and after conditioning (Fig. 1*H*). In this matrix, diagonal boxes represent test stimulus-evoked spiking at the stimulated RA ("self-activated") and off-diagonal boxes represent those at other RAs

("heteroactivated"). The difference matrix of this particular example showed an overall increase in the spiking response at all coactivated RAs. The results from 12 mice were summarized by plotting the total spike counts over the 30-ms period immediately following the test stimulus onset (Fig. 1 *I* and *J*).

In parallel control experiments (on six mice), instead of coactivation, we activated the RAs at a random sequence within each burst stimulation (generated by random permutation of the sequence, pulse duration 16.7 ms), with constant intervals (16.7 ms, 15 Hz) between sequential stimuli and the same total number of stimuli at each RA as that used for the coactivation experiments described above (*SI Appendix*, Fig. S2*A*). We found that such random sequence activation failed to cause any significant change in spiking evoked by test stimuli at all RAs (*SI Appendix*, Fig. S2 *B–D*). Finally, we monitored the spontaneous spiking rates at both coactivated and noncoactivated units during the 30-ms period before the test stimulation, and found that the spontaneous spiking rate remained unchanged throughout the experiments (*SI Appendix*, Fig. S3*A*), indicating stable multiunit recording over time. Results from 13 mice were summarized by plotting the average spontaneous spiking rate during a 10-min period before and after coactivation (*SI Appendix*, Fig. S3*B*). The results showed no significant change in the spiking rates, suggesting that the enhanced spiking of neuronal groups in response to test stimuli was due to enhanced neuronal excitation in response to test stimuli. Taken together, these results indicate that synchronous coactivation of cortical neurons is required for the observed enhancement of light-evoked neuronal firing.

Role of Synaptic Transmission in Optogenetically Evoked Responses.

Two findings support the idea that the test light-evoked spiking detected by the electrodes for other RAs resulted from synaptic connections from self-activated neurons directly to heteroactivated neurons. First, we found that the infusion of CNQX (6-cyano-7-nitroquinoxaline-2,3-dione; 0.5 mM), an antagonist of the AMPA (α-amino-3-hydroxy-5-methyl-4-isoxazolepropionic acid) subtype of glutamate receptors, led to a marked reduction of test-evoked spiking of heteroactivated groups. As shown by the example recording (Fig. 1*K*), evoked spiking of self-activated neurons was greatly reduced, whereas those at heteroactivated neurons were essentially all eliminated. The results from all CNQX experiments ($n = 8$ mice) showed a significant reduction of the average spiking for both self- and heteroactivated groups (Fig. 1 *K*, *Bottom*). At many RAs, substantial spiking could still be evoked by the test light after the CNQX treatment. This may be caused by direct light-evoked neuronal firing independent of synaptic transmission, including activation of spiking at the soma and axonal/dendritic processes. Second, whole-cell recording of excitatory postsynaptic potentials (EPSPs) in neurons of heteroactivated groups revealed a range of synaptic delay (3.4 to 14.5 ms, 4.9 ± 1.0 ms, $n = 8$) following the light onset, consistent with the existence of both mono- and polysynaptic connections (Fig. 1*L*). The EPSP onset was defined as the time when the mean membrane potential exceeded three times the SD from the baseline. Thus, the present optogenetic approach allowed us to examine synaptic connectivity among distant neuronal groups within the cortex.

Further Characterization of the Enhancement Effect.

Further experiments were performed to characterize the enhancement of test stimulus-evoked neuronal spiking induced by coactivation of cortical neurons. First, we examined the persistence of the enhancement effect by monitoring the changes in cortical neuronal spiking induced by the test stimuli at different times following repetitive coactivation (Fig. 2*A*). We found that the enhancement of the spiking in coactivated units persisted for as long as the experiments were performed, up to 100 min after coactivation. Second, we examined the effect of repeated episodes of coactivation on the enhancement of evoked spiking. We found

www.manaraa.com

that the enhancement effect quickly reached a plateau after three episodes of coactivation applied at 30-min intervals (Fig. 2B). This saturability is reminiscent of activity-induced long-term potentiation (LTP) of excitatory synapses (17). Third, we tested the dependence of the enhancement effect on the total number of coactivation stimuli and found that progressive reduction of the total number of bursts (at 30 Hz, 1-s burst interval, 5 pulses per burst) resulted in a gradual reduction of the enhancement (Fig. 2C), with no detectable enhancement below 15 bursts. Fourth, we examined whether the enhancement effect depends on the size of the neuronal population coactivated. We varied the number of coactivated RAs from one to four in different mice that were similarly ChR2-transfected in V1, and found significant elevation of evoked spiking when the coactivation was applied to four RAs, but not to three, two, or one RA (Fig. 2D). We also found that the enhancement effect depends on the bursting pattern of coactivation stimuli, since tonic coactivation at 5 or 0.05 Hz, with the same total number (250) and pulse duration (16.7 ms) of light stimuli, was much less effective in inducing the enhancement effect (Fig. 2E). Thus, the enhancement effect was long-lasting and saturable, and required coactivation of a large number of cortical neurons in the same cortical area at a sufficiently

high frequency and repetition, properties reminiscent of LTP found at many central synapses.

We also examined whether such a coactivation effect is specific to sensory cortices. By the same virally induced expression of ChR2 and multielectrode array recording in the mouse motor cortex (M1/M2), we found the same repetitive-burst light stimuli as that described above resulted in similar coactivation-induced enhancement of the evoked spiking in the motor cortex (Fig. 2F), suggesting that the enhancement is a general property of the cerebral cortex. Finally, we found an interesting nonlocal effect of coactivation. By coactivating four RAs in V1, we found test light applied to noncoactivated RAs located more than 1 mm away also evoked higher spiking (Fig. 2G), suggesting the long-range spread of the enhancement effect, a phenomenon that was further explored in later experiments (see below).

Synaptic Mechanisms Underlying the Enhancement Effect. To further elucidate potential mechanisms underlying the effect of repetitive coactivation on test stimulus-evoked cortical neuronal spiking, we examined the involvement of long-term synaptic potentiation in the observed enhancement of neuronal spiking following repetitive
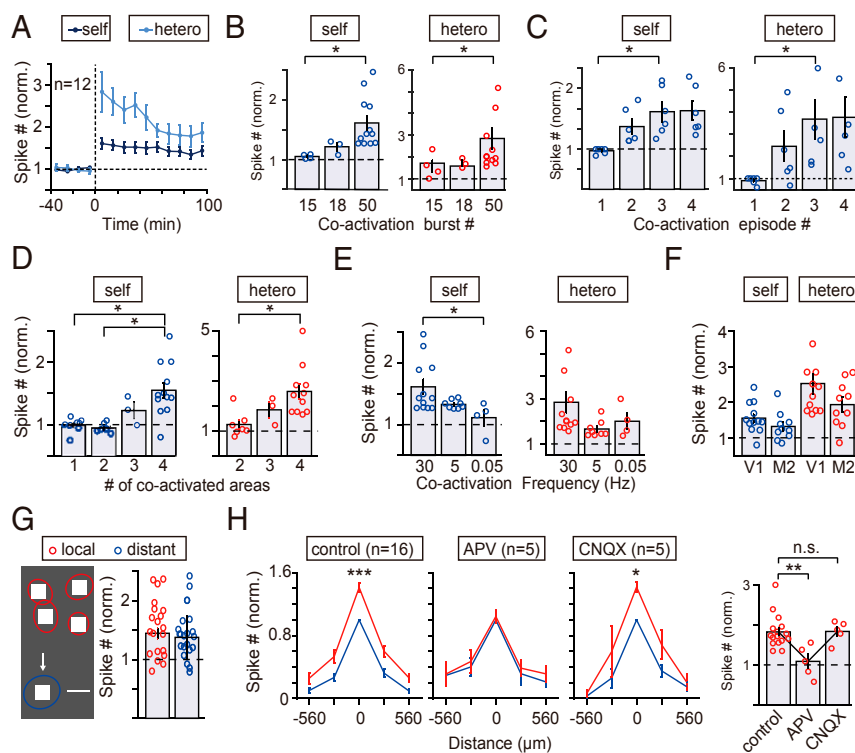

Fig. 2. Characterization of enhanced excitability induced by coactivation. (A) Time course of the enhancement. Mean test-evoked spiking responses (normalized by the response before coactivation) with time after coactivation (t = 0; duration 50 s), for self- and heteroactivated groups. Data represent mean ± SEM (n = 5 mice). (B) Dependence of the enhancement on the total burst number during coactivation for self-activated (Left) and heteroactivated (Right) groups. Each burst consists of five pulses at 30 Hz (pulse duration 16.7 ms). Data are represented as in A (*P < 0.01, t test; n, number of mice). (C) Enhancement effects after each of three episodes of coactivation. Average test-evoked spiking rates prior to the first coactivation (0) and after each of the successive episodes of coactivation (1 to 3), for self-activated RA. (D) Effects induced by different numbers of coactivated areas. Data are presented and statistics are the same as in C (*P < 0.01, t test; number of mice used, 8, 7, 4, and 12, respectively, for one to four areas coactivated). (E) The effect of the coactivation frequency on the enhancement. The same total number of coactivating stimuli was applied at different frequencies. Data are presented and statistics are as in C (*P < 0.05, t test; number of mice used, 12, 8, and 4, respectively, for 30, 5, and 0.05 Hz). (F) Coactivation induced a similar enhancement effect in self-activated (blue dots) and heteroactivated (red dots) areas in visual and motor cortices (P > 0.1, t test). (G) Effects at coactivated areas and distant noncoactivated areas. (G, Left) Diagram depicting four coactivated RAs (red circles) and one distant RA not coactivated (blue circle) in one example experiment. White squares, optogenetic stimulation spots. (Scale bar, 200 μm.) (G, Right) Enhancement effects at coactivated and distant noncoactivated RAs. The difference is not significant (P > 0.8, t test; n = 22 mice). (H) Effects of test stimulus-evoked spiking in mouse V1, in three groups of mice under perfusion of artificial cerebrospinal fluid (ACSF) (control; Left), ACSF containing CNQX (50 μM; Right), and ACSF containing APV (500 μM; Middle). The enhancement in evoked spiking rates, normalized by that at the self-activated RA (at 0), are plotted for both self-activated and adjacent heteroactivated (at 280 and 560 μm) RAs. Histograms (Right) summarize the enhancement effects at the self-activated RAs for data from three types of treatments. Data represent mean ± SEM (*P < 0.05, **P < 0.01, ***P < 0.001, t test; n.s., not significant; n, number of mice).

Zhang et al.

coactivation of large populations of cortical neurons in V1. Since LTP of most central synapses requires the activation of the NMDA subtype of glutamate receptors (18), we perfused the exposed V1 with the NMDA receptor antagonist D-2-amino-5-phosphono-pentanoic acid (APV; 500 μM) for 30 min prior to and during the experiment. We found that the enhanced test stimulus-evoked spiking was largely abolished by the APV perfusion (Fig. 2H). Furthermore, as shown in the example case in *SI Appendix*, Fig. S3, coactivation further induced the enhancement effect 2 h after APV washout. This feature is consistent with NMDA receptor-dependent LTP of synaptic connections induced by coactivation.

In the above experiments, blocking NMDA receptors also led to a significant reduction (41 ± 4%, n = 24) in the spontaneous neuronal firing rate (*SI Appendix*, Fig. S3C). To test the possibility that the failure in observing the conditioning effect was caused by a general reduction in the cortical spiking rather than a specific blockade of LTP, we perfused the cortex with a low concentration of the AMPA receptor antagonist CNQX (50 μM) as an independent approach to reduce neuronal spiking. We found that when reduction (39 ± 8%, n = 4 mice) in cortical firing was induced by blocking AMPA receptors with CNQX perfusion, significant enhancement of the spiking responses remained (Fig. 2H). These results support the notion that the activation of NMDA receptors is required for the induction of the enhancement effect.

The enhanced spiking responses may result from LTP-like potentiation of synaptic efficacy or increased intrinsic neuronal excitability, or both. To measure changes in synaptic responses, we directly measured test stimulus-evoked EPSPs using in vivo whole-cell recording. In these experiments, we first determined the RA of a single V1 neuron by recording EPSPs and action potentials evoked by sequential blue-light spot stimuli (size 130 × 130 μm, duration 80 ms) at random locations on the V1 surface (Fig. 3A). We found that RAs of single neurons covered 306 ± 11 μm in radius at the standard light intensity (Fig. 3 A, *Inset* and *Materials and Methods*), and the spatial temporal structure of RAs was stable for at least 2 h (*SI Appendix*, Fig. S4). We then applied the coactivation in the same pattern as described above by simultaneous light-spot activation of four nearby V1 regions, one of which was the RA of the recorded neuron (Fig. 3B). The test stimulus-evoked EPSPs (with action potentials truncated if present) were measured by applying test stimuli at different distances from the recorded neuron. Based on the onset latency of the depolarization, the test stimulus closest to the recorded neuron could evoke monosynaptic EPSPs, whereas stimuli applied at more distant areas evoked mono- or polysynaptic EPSPs with a delayed onset of 3.4 to 14.5 ms (Fig. 1L). As shown in the example neuron, repetitive coactivation increased the amplitude of both mono- and polysynaptic EPSPs (Fig. 3 B–D). Overall, the mean EPSP amplitude (averaged over 50 test trials after coactivation) in the recorded neurons increased significantly after coactivation to a level 210 ± 10% (n = 6; SEM) of the baseline value (averaged over 50 test trials before coactivation) (Fig. 3C). Furthermore, the enhancement of EPSP amplitude was reduced to 150 ± 6% (n = 3; SEM) of the baseline value in mice that were infused with APV (500 μM) 30 min before and during the experiment (Fig. 3D). In addition, we found no significant modification of the input resistance and membrane time constant of the local coactivated neurons and distant noncoactivated neurons (*SI Appendix*, Fig. S5). Thus, coactivation of a large population of neurons may have potentiated synaptic transmission.

Repetitive optogenetic activation of subcortical neurons elicited a brain-wide spread of blood oxygen level-dependent signal (19–21), suggesting local coactivation of large populations of neurons may cause neuronal excitation at distant regions. In our study, we found an enhanced test stimulus-evoked neuronal excitation at cortical regions that were not coactivated and exhibited no spiking responses during coactivation. However, the coactivation may have evoked subthreshold neuronal depolarization in distant regions that caused the distant effect. Indeed, in vivo whole-cell recording revealed significant membrane depolarizations in V1 neurons located in regions not coactivated (2 mm away for the example neuron in Fig. 3 E and F), with the average latency of onset (56.6 ± 17.6 ms, n = 6) much longer than those observed in neurons at coactivated regions (3.9 ± 0.5 ms, n = 6). These results suggest that the repetitive coactivation of cortical neurons may cause membrane depolarization in distant cortical regions, mediated by mechanisms involving polysynaptic transmission.

Cross-Cortical Spread of Spiking Enhancement. The nonlocal effects of coactivation found in the above experiments prompted us to ask whether the enhancement effect could spread to other cortical areas. We first infected V1 and S1 of the mouse with viral vectors expressing ChR2 in pyramidal neurons and examined whether repetitive coactivation of neurons in V1 could affect evoked spiking in S1, and vice versa. In the example experiment shown in Fig. 4A, coactivation was applied to four linearly aligned RAs (areas 1 to 4) in S1, and cortical responses to the test stimuli were recorded before and after coactivation, for both coactivated RAs (1 to 4) in S1 and noncoactivated RAs (5 and 6) in V1. Although no obvious evoked spiking was observed in V1 during the coactivation applied to S1 (Fig. 4B), test stimulus-evoked spiking was elevated both in the coactivated and non-coactivated RAs (Fig. 4C). The results were summarized by the difference matrix, which measured the spiking enhancement at all RAs when the test stimulation was applied sequentially to each RA (Fig. 4D), and we found that for the above example experiment that self-activated spiking was enhanced for test stimulation at all RAs (diagonal), and heteroactivated spiking (off-diagonal) was elevated not only for RAs that were coactivated but also for RAs that were not coactivated. Thus, spiking enhancement could spread to distant cortical regions that were not coactivated.

Results from all mice (n = 4) are summarized in Fig. 4 E and F. Significant elevation of test stimulus-evoked spiking was found at both coactivated and noncoactivated areas after coactivation of four RAs at either S1 or V1. In contrast, no enhancement effect was found when coactivation was applied to only two RAs in either V1 or S1, suggesting that the enhancement effect may depend on the size of the coactivated neuronal population.

We further analyzed the enhancement of spiking responses within local cortical regions quantitatively by using the test stimulus to evoke spiking at neighboring cortical regions. The cortical region covers the recording site of seven neighboring electrodes. One of them was under the test stimulus and this site was termed self-activated. Other electrodes were distributed equally on two sides of the test stimulus. These sites were termed heteroactivated. We found that the self-activated spiking response was highest, and heteroactivated responses were all elevated, with progressive reduction of the total spike numbers for electrodes at larger distances (within ~450 μm) from the stimulated RA (marked as 0 μm, Fig. 4G). This result was observed in both the coactivated cortex (S1) and the noncoactivated cortex (V1). This analysis provided the response profile for both self-activated and heteroactivated areas at the same time and revealed the overall change of the test stimulus-evoked spiking after coactivation at the local cortical area. Summary of the response profiles from all four mice examined indicates that the enhancement effect on heteroactivated spiking depends on their distances from the test-stimulated RA, regardless of whether the latter was coactivated (Fig. 4H).

Enhancement Depends on the Size of the Coactivated Population. Having found that the spiking enhancement due to the coactivation of cortical neurons could spread to nearby cortices, we further examined whether the enhancement effect depends on
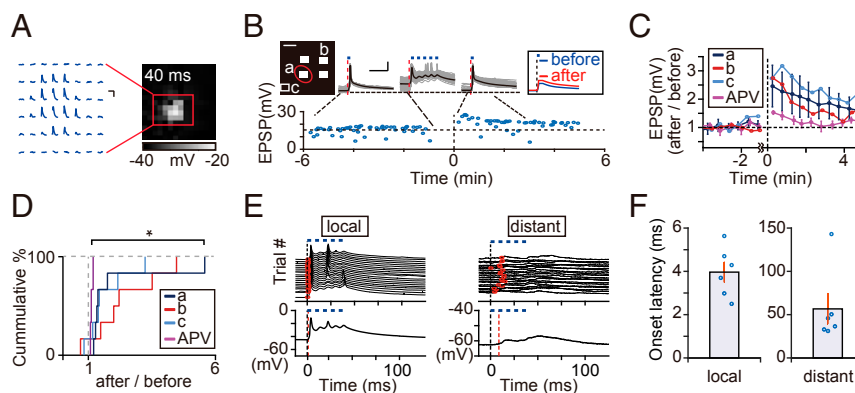
www.manaraa.com

Fig. 3. Synaptic potentiation resulting from coactivation. (*A*) Mapping of the RA of a single V1 neuron for optogenetic stimuli that evoked depolarization responses, recorded by in vivo whole-cell recording. Traces shown are responses of an example neuron evoked by light stimuli at 48 different locations (spacing 130 μm). The map (*Right*) depicts the response area of the recorded neuron (red box), based on the amplitude of stimulus-evoked depolarization at 40 ms after stimulus onset (coded in grayscale shown below). Histograms show the distribution of the radius of RAs for all neurons recorded (mean 306 ± 11 μm, SEM; n = 31). (Scale bars, 150 ms, 10 mV.) (*B*) Membrane potential changes of an example neuron throughout the coactivation experiment. Data points represent the depolarization amplitude (with action potentials truncated), evoked by the same test stimulus before and after coactivation. The map above shows areas of coactivation (four white spots) and test stimulation (a and b, coactivated; c, not coactivated). Elliptical contour, Gaussian fit at 1 SD, indicating the RA of the recorded neuron. Traces above show membrane potential changes evoked by test stimuli before, during, and after coactivation. Gray traces, 50 individual trials; black traces, averages. Red dashed lines, light onset. Black horizontal dashed lines, −70 mV. Boxed traces, average traces of membrane depolarization before (blue) and after coactivation. (Scale bars, 70 ms, 20 mV.) (*C*) Time course of the coactivation effect of all recorded neurons. Averaged amplitude (over five trials) of test-evoked depolarization (action potentials truncated, normalized by the mean value before coactivation) before and after coactivation. a, b, and c, experiments with test stimuli applied to three different areas (marked as a, b, and c in *B* above). APV, experiments using a perfusion of APV (500 μM; n = 3), with test stimuli at position "a." (*D*) Cumulative percentage plot of the extent of potentiation. Mean EPSP amplitude of the first five test trials after coactivation was normalized by that before coactivation. The differences between results obtained with and without APV treatment were significant for tests at position "a" (1.5 ∼ 2 min after coactivation; *P = 0.01, Kolmogorov–Smirnov test). (*E*) Membrane depolarizations of the neuron coactivated (local) and not coactivated (distant) during the period of repetitive coactivation, shown for sequential trials (*Top*) and the average over 50 trials (*Bottom*). (*F*) Onset time of membrane depolarization in response to coactivation for neurons coactivated (local, 3.9 ± 0.5 ms; n = 6 from four mice) or not coactivated (distant, 56.6 ± 17.6 ms; n = 6 from four mice).

the size of the coactivated neuronal population and/or the distance between coactivated and tested areas. In these experiments, multiple electrode arrays were implanted along a line perpendicular (n = 4) or parallel (n = 3) to the midline, covering V1 and adjacent cortical areas (Fig. 5*A*). Single light spots of increasing sizes were used to repetitively coactivate neurons within one RA (RA1), with the maximal size equivalent to the total area activated at four RAs in the earlier experiments described above. Coactivation-induced changes in the test stimulus-evoked responses were measured at RA5 or RA6 along the long axis of the electrode arrays over 2- to 3-mm distances. Fig. 5*B* depicts the results from one example experiment (with the largest light spot used at RA1). We found that, although neuronal spiking evoked by RA1 activation decreased with distance during coactivation, test-evoked spiking responses were enhanced at all RAs, as shown by the elevated PSTH profiles and total spike numbers (Fig. 5*B*).

Results from all seven mice are summarized in Fig. 5*C*. The extent of the enhancement effect was quantified by the ratio of total test-evoked spike number (within the 30-ms window after test stimulus onset) after vs. before coactivation. We found that the enhancement ratio was significantly above 1 for all RAs when the area of coactivation was ∼0.08 mm². A smaller area of coactivation at ∼0.06 mm² also resulted in some enhancement at RAs closer to the coactivated RA1. The population-size dependence of the enhancement effect is summarized in Fig. 5*D*, which shows that coactivation of sufficiently large populations of neurons was required for inducing enhanced neuronal spiking. In these experiments, neurons could be stably activated by the test light spot with a light intensity above 50% of the maximal intensity (*SI Appendix*, Figs. S1 and S7*B*). We estimated that the total number of ChR2-expressing neurons activated by the standard test light spot (one RA) at the cortex was ∼6,000 neurons (*Materials and Methods*). The total number of neurons

required to reliably induce enhanced neuronal spiking (four RAs) was thus estimated to be on the order of a few thousand, within a cortical volume with a diameter of about ∼1 mm (*SI Appendix*, Fig. S7*B*).

Cooperativity among Distant Coactivated Neuronal Populations. We next inquired whether the enhancement depends on the spatial distribution of coactivated areas. We coactivated four RAs that were located in two different cortices of the same hemisphere. Interestingly, whereas two RAs coactivated in either V1 or S1 alone had no enhancement effect on test-evoked neuronal spiking (Fig. 4*H*), coactivating two RAs in V1 and two RAs in S1 simultaneously induced elevation of evoked spiking, as shown by the spike raster and PSTH from the example experiment (*SI Appendix*, Fig. S6*A*). A similar enhancement effect was also found for coactivation of three RAs in V1 and one RA in S1, or vice versa (*SI Appendix*, Fig. S6 *B–D*), whereas three-RA coactivation in one cortex alone induced only a weak enhancement effect (Fig. 6*B*). These results are in agreement with the previous data on the dependence of coactivation effects on the size of the area coactivated, as shown by overlaying the averaged normalized after/before ratio of the spiking responses resulting from coactivation of two, three, and four RAs onto a previous plot of the area-size dependence (Fig. 5*D*). Together, these findings indicate the importance of the overall size of the coactivated neuronal population in enhancing neuronal excitation regardless of whether the coactivated neurons are distributed within one cortex or in different cortices, in support of the notion of cooperativity among distant neuronal populations in the induction of the enhancement effect.

We also addressed the issue of whether similar enhancement effects could be induced in mice in the absence of anesthesia. As shown by the example in Fig. 6*A*, we coactivated four RAs that were located in two different cortices in the same hemispheres of
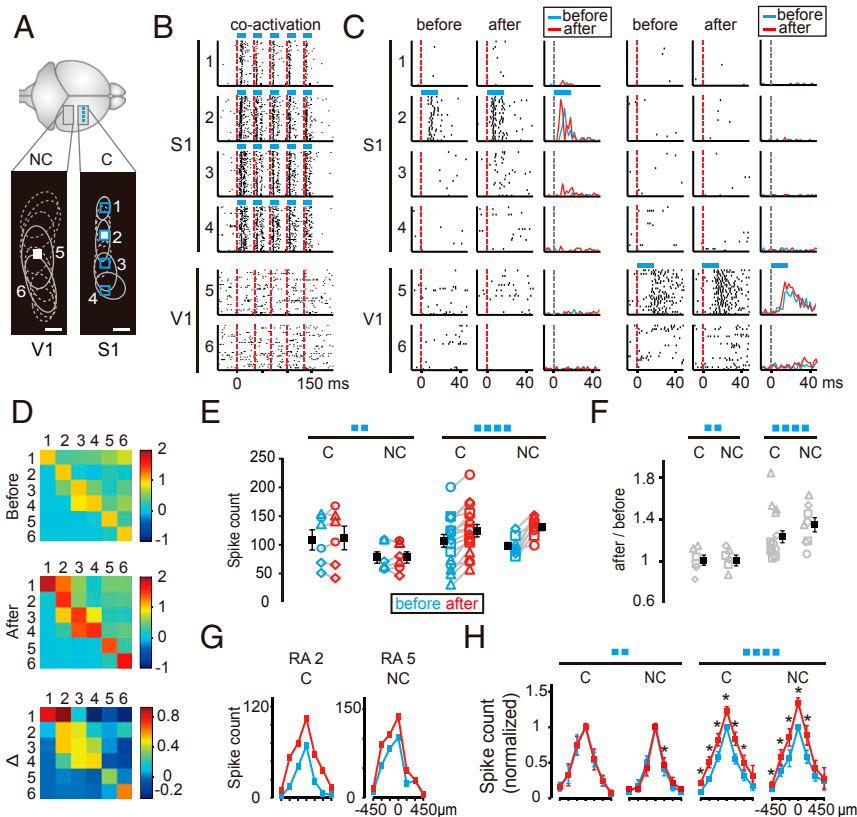
Zhang et al.

www.manaraa.com

Fig. 4. Cross-cortical spread of spiking enhancement. (*A*) Schematic diagram depicting recorded areas (1 to 6) and coactivated areas (1 to 4) in an example experiment. Gray circles, tested (solid) and untested (dashed) RAs; white squares, test spots at areas not coactivated (NC) in V1 and the coactivation area (C) in S1; blue squares, coactivation sites. (Scale bars, 300 μm.) (*B*) Data from the experiment depicted in *A*. Peristimulus raster plots over 50 trials during coactivation, showing spike trains at six RAs in response to coactivation. Red dashed line, light stimulus onset. Blue bar, light stimulation (16.7 ms). (*C*) Data from the same experiment as in *B*. Peristimulus raster plots and peristimulus time histogram (spike counts in 2-ms bins, range 0 to 25 spikes) of spike trains over 50 trials in six RAs, in response to test stimuli (16.7 ms; blue bar) applied to RA2 (*Left*) and RA5 (*Right*), before and after coactivation. Gray and red dashed lines, test stimulus onset. (*D*) Summary of changes in spiking responses in all six tested RAs in the above experiment, evoked by test stimulation applied to all RAs. (*D*, *Top* and *Middle*) Color-coded average evoked spiking rate for the first 30-ms poststimulus onset, before and after coactivation, all normalized by that of self-activated spiking (diagonal values) before coactivation. (*D*, *Bottom*) Differences of normalized spiking responses (Δ = after − before). (*E*) Pairwise comparison of spiking responses at all RAs, for self-activated responses in the coactivation area (C) and in areas not coactivated, before (blue) and after coactivation of two or four RAs (marked by blue squares). Data points represent spike counts recorded within the first 30 ms after stimulus onset in response to test stimulation at its own RA; different data symbols represent different mice ($n = 3$). (*F*) Enhancement of spiking responses represented by the ratio of spike counts after vs. before coactivation, for the dataset in *E*. Different gray symbols represent different mice. Black points represent the mean ± SEM. (*G*) Response profiles for test stimulation at RA2 (coactivated) and RA5 (not coactivated and located in a different cortex). Spike counts for each RA at different distances from the self-stimulated RA. (*H*) Summary of the enhancement of response profiles for the two-RA and four-RA coactivation, for responses at C and NC areas, normalized by that at self-activated RAs before coactivation. Data represent mean ± SEM (*$P < 0.05$, paired *t* test for data at the same distance).

unanesthetized mice, and found the enhancement effect of coactivation in both spiking raster and PSTH. A summary of the response profiles before and after four-RA coactivation of V1 and S1 ($n = 3$ mice; Fig. 6*C*) showed that the enhancement effects were similar to those found in anesthetized mice, with the after/before spike count ratios showing a similar tendency of enhancement in mice with and without anesthesia, with the highest level of enhanced spiking at self-activated RAs and lower levels at heteroactivated RAs.

Cross-Hemispheric Spread and Cooperativity of Spiking Enhancement. Using unanesthetized mice, we further examined whether the enhancement effects of repetitive coactivation of cortical neurons in one hemisphere could lead to excitability changes in the contralateral hemisphere. We transfected both hemispheres with viral vectors expressing ChR2 in pyramidal neurons and recorded light-evoked neuronal responses with multielectrode arrays implanted in both hemispheres. In the experiment (*SI Appendix*, Fig. S6*E*), we repetitively coactivated four RAs in the visual area of the left hemisphere, and found that neuronal spiking responses

evoked by the test light stimuli were elevated in the visual areas of both hemispheres, as shown by the spiking rasters and PSTH (*SI Appendix*, Fig. S6 *F* and *G*). The spiking profiles from all experiments ($n = 3$ mice) are summarized in Fig. 6 *D*, *Left*. Furthermore, the extent of enhancement in both hemispheres was similar (*SI Appendix*, Fig. S6*H*). Similar experiments were also carried out on anesthetized mice. We found repetitive coactivation of four RAs in V1 of one hemisphere could enhance the test stimulus-evoked spiking of S1 neurons in the contralateral hemisphere (Fig. 6 *D*, *Middle*; $n = 4$ mice).

We also examined cross-hemispheric cooperativity in inducing spiking enhancement by coactivating neuronal populations located in two hemispheres of unanesthetized mice (Fig. 6 *D*, *Right*). Repetitive coactivation of two RAs in V1 of each hemisphere also caused enhancement of evoked responses (Fig. 6 *D*, *Right*). The averaged light-evoked spiking profile from coactivation of two RAs in either hemisphere showed very little effect in enhancing the evoked neuronal responses. Together with the findings on coactivation in only one hemisphere, these results support the notion of cross-hemispheric cooperativity of neuronal
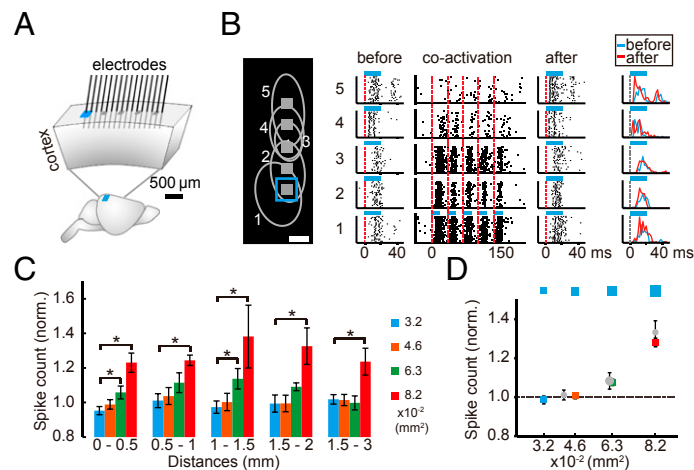
Fig. 5. Dependence on the size of the coactivated area. (*A*) Schematic diagram for the coactivated (blue square) and recorded areas. Gray squares, test spots at different distances from the coactivation area. (*B*) Data from an example experiment. (*B*, *Left*) The relative size and position of RAs (gray circles), test stimulation spots (gray squares), and coactivated area (blue square). (*B*, *Middle*) Peristimulus raster plots of spike trains in five RAs over 50 trials, in response to test stimuli (blue bar) applied to each RA before, during, and after coactivation. Red dashed line, test stimulus onset. (*B*, *Right*) PSTH of test stimulus-evoked responses before and after coactivation. Gray dashed line, stimulus onset. (Scale bar, 200 μm.) (*C*) Summary of the enhancement of evoked responses for all experiments after coactivation, normalized by that before coactivation, at different recording sites. Different colors correspond to data obtained by using different sizes of the coactivated area, grouped by their distances to the coactivated area (*$P < 0.05$, paired t test; $n = 3$ or 4 mice). (*D*) Summary of the enhancement of evoked responses for all experiments shown in *C* (colored) and in Fig. 6*C*. Data represent mean ± SEM.

activation, leading to global enhancement of neuronal excitability when a sufficiently large population of cortical neurons is coactivated.

Inhibiting the Midline/Intralaminar Thalamus Reduced the Enhancement Effect. Light illumination on the cortex not only activated local cortical neurons but also indirectly activated neurons in other cortical regions via subcortical recurrent circuits. By implanting linear multielectrode arrays (eight electrodes at 500-μm spacing) into the subcortical regions of the mouse brain (depth up to ~3 mm), we observed neuronal spiking in the thalamus and striatum that correlated with cortical coactivation with different sizes of light spots (*SI Appendix*, Fig. S8*A*). To further identify subcortical brain regions that were activated during repetitive cortical coactivation, we examined c-Fos immunostaining of mouse brain slices obtained at ~40 min after repetitive coactivation of four RAs in V1. As shown by the example section (*SI Appendix*, Fig. S8*B*), we observed distinct c-Fos signals in the midline/intralaminar thalamus besides widespread c-Fos+ neurons in the cortex, suggesting the involvement of neurons in this area during coactivation.

Neurons in the midline/intralaminar thalamus send diffuse axon projections to the cerebral cortex and striatum (22). Functional brain imaging studies showed that optogenetic stimulation of the central thalamus (including the midline/intralaminar thalamus) induced widespread cortical excitation (21). The midline/intralaminar thalamus has been postulated to play a critical role in regulating arousal and attention (23). Lesion of the midline/intralaminar thalamus reduces cortical activation (24–27). We thus tested the potential involvement of midline/intralaminar thalamus activation in the enhancement of global neuronal excitability in the cortex induced by repetitive coactivation.

We used a chemogenetic method to inhibit neuronal activity in the midline/intralaminar thalamus. This was achieved by expressing the designer receptor which is exclusively activated by a designer drug (28). In addition to the standard injection of the AAV vector that expresses ChR2-2a-mCherry in the visual cortex (V1), we also injected an AAV vector that expresses hemagglutinin (HA)-hM4D-IRES-mCitrine under the human synapsin (hSyn) promoter in the midline/intralaminar thalamus (Fig. 7*A*). Four weeks after viral injection, we intraperitoneally administered clozapine-*N*-oxide (CNO) that is known to inhibit the activity of hM4D-expressing

neurons to the injected mice. When repetitive coactivation of four RAs in V1 was applied in the same manner as that described above (Fig. 1*F*), we found that the enhancement of test stimulus-evoked spiking of cortical neurons was largely abolished in the self-activated RAs and markedly reduced in the nearby heteroactivated RAs ($n = 4$; Fig. 7*B*), whereas the enhancement effect was not affected in control mice injected with saline ($n = 3$; Fig. 7*B*). We also injected the same virus into the brain region about 1 mm posterior to the midline/intralaminar thalamus to examine whether other thalamic regions were involved. The summary result from three mice (Fig. 7*B*) showed reduced enhancement effects in both self-activated and heteroactivated RAs after the coactivation of four RAs in V1. Due to the limitation of the experimental protocol (slow action of peritoneally applied CNO), we could not examine the effect of CNO on neuronal responses to test stimuli (as compared with the saline control). Thus, it remains possible that there was some nonspecific effect of CNO on the coactivation-induced spiking enhancement in both thalamic regions. Nevertheless, the different inhibition effect at the "self-stimulation" (0-μm) site supports the importance of the midline/intralaminar thalamus, even in the presence of some nonspecific CNO effect. This result suggests that the activity of the midline/intralaminar thalamic neurons contributed more to the enhancement effect induced by coactivation in V1 than other thalamic regions. The coactivation-induced activity of thalamic neurons may be required for the enhancement of cortical excitability via their feedback facilitation of cortical neuronal excitation, and for the global spread of the enhancement effect via their diffuse cortical projections.

Discussion

In this study, we used DMD-based optogenetic stimulation that allows defined spatiotemporal manipulation of spiking activities in large populations of cortical neurons. We showed that repetitive coactivation of a large population of cortical neurons results in persistent enhancement of neuronal spiking evoked by optogenetic stimulation. Such an effect was saturable after several repeated episodes of coactivation, and depended on NMDA receptor activation. In vivo whole-cell recording of neuronal responses further showed that this coactivation-induced enhancement is accompanied
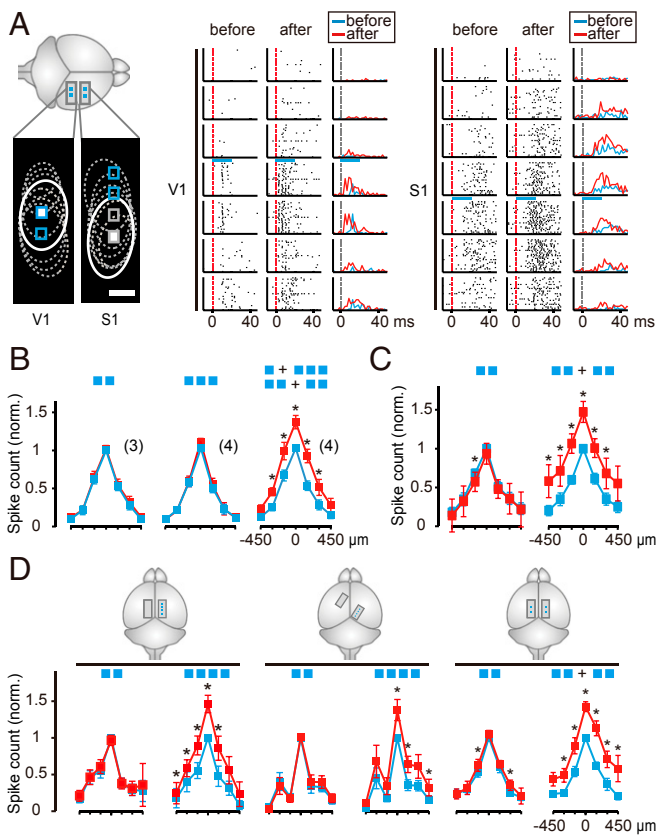
Zhang et al.

NEUROSCIENCE

Fig. 6. Cooperativity among distant coactivated neuronal populations in anesthetized and awake mice. (A) Enhancement of evoked responses following coactivation of neurons in distant cortical regions in an awake mouse. (A, Left) Schematic diagram showing coactivating areas. Dashed circles, RAs for the multielectrodes in two cortical regions. Solid circles, tested RAs; white squares, testing light spots in this example experiment; blue squares, coactivated areas. (Scale bar, 300 μm.) (A, Right) Examples of peristimulus raster plots and PSTH of spike trains in seven RAs in each cortical region (V1 and S1), in response to 50 trials of test stimuli (white squares) applied to two example RAs (white circles) before and after coactivation. Red and gray dashed lines, stimulus onset; blue bar, duration of test stimulation. (B and C) Summary of the evoked response profiles from all experiments on anesthetized (C) and awake mice (D), following coactivation in distant cortical regions, for experiments using coactivation of two, three, or four RAs. For coactivation of four RAs, data were collected from experiments involving an unequal number (1/2) and an equal number (2/2) of coactivated RAs in distant cortical regions, as marked by the blue squares above. Data points represent mean ± SEM (*P < 0.05, paired t test; the number of mice is shown in parentheses). (D) Summary of experiments involving different locations of test RAs and coactivated RAs. (D, Left) Coactivation in ipsilateral and test in contralateral V1 (n = 3 awake mice), for coactivation of two or four RAs. (D, Middle) Similar to D, Left, except test RAs were in contralateral S1 (n = 4 anesthetized mice). (D, Right) Coactivation of two RAs in V1 of each hemisphere (n = 3 awake mice). Data points represent mean ± SEM (*P < 0.05, paired t test).

by an NMDA receptor-dependent increase in the amplitude of excitatory postsynaptic potentials. These features are consistent with the induction of activity-dependent LTP. Importantly, such an enhancement effect required the repetitive coactivation of a sufficiently large population of cortical neurons, which could be distributed either in one local cortical area or in distant cortical areas that could even be located in different hemispheres. Finally, we showed that neuronal activity in the midline/intralaminar thalamus may be involved in the enhancement of cortical excitability. Our results support the notion that repetitive correlated firing of a sufficiently large population of cortical neurons triggers long-range

cortical and subcortical cooperative interaction in neuronal excitation, leading to global enhancement of cortical excitability.

Cellular Mechanisms Underlying Enhanced Neuronal Excitation. Repetitive correlated neuronal firing is known to result in LTP at many excitatory synapses in the brain, leading to elevated postsynaptic excitation. Our results indicate that coactivation of a large population of cortical neurons induced persistent elevation of neuronal spiking in response to test optogenetic stimulation. Such increased neuronal excitation could result from potentiation of intracortical synaptic connections or elevated intrinsic excitability of cortical neurons, or both. We found that an increase in both EPSP amplitude and evoked spiking after coactivation depended on NMDA receptor activation, and the enhancement effect was also observed in brain regions not coactivated (Figs. 2G and 4H). Thus, coactivation-induced synaptic potentiation is likely to provide the major contribution to the elevated neuronal spiking, although elevated intrinsic neuronal excitability in either pre- or postsynaptic neurons (29, 30) could not be excluded.

Hebbian Potentiation of Neuronal Excitability. A recent study showed that after repetitive optogenetic coactivation of a group of V1 neurons within a local cortical area (240 × 240 μm), optogenetic stimulation of a single neuron in the coactivated group could persistently activate more neurons in the local cortical area (10). Using glutamate uncaging to excite individual neurons in the mouse barrel cortex, Kim et al. (11) found that after repetitive sequential activation of a sufficient number of neurons, spiking responses evoked by test glutamate stimuli on both conditioned and unconditioned neurons were persistently elevated. Our finding is consistent with these previous findings. Furthermore, we showed that the enhancement of cortical excitability is global, including the unstimulated contralateral cortex when a sufficiently large population of cortical neurons was coactivated locally. However, in the study of Carrillo-Reid et al. (10), there was no enhanced excitation for visual stimulus (grating)-evoked neurons. This discrepancy may be attributed to the difference in the number of neurons and circuits excited by optogenetic vs. visual stimulation.

Number of Neurons Activated during Repetitive Coactivation. The finding that the enhancement effect depended on the number of the coactivated cortical neurons was based on the requirement of the total cortical area optogenetically stimulated, using similar
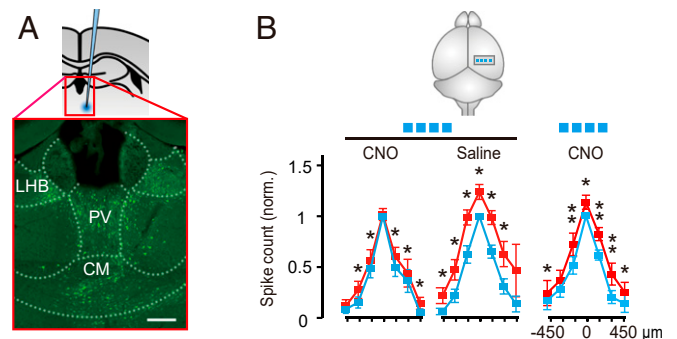

Fig. 7. Involvement of the midline/intralaminar thalamus. (A) Expression of hM4D at the midline/intralaminar thalamus. (A, Left) Schematic diagram showing the virus injection site. (A) Fluorescent image of hM4D-positive cells. CM, central medial thalamic nucleus; LHB, lateral habenular nucleus; PV, paraventricular thalamic nucleus. AAV vector, hSyn-HA-hM4D-IRES-mCitrine. (Scale bar, 200 μm.) (B) Summary of experiments involving coactivation of four RAs in V1 at 30 min after intraperitoneal injection of CNO or saline in mice that expressed hM4D in (Left, n = 3 mice and Middle, n = 3 mice) or about 1 mm posterior to (Right, n = 4 mice) the midline/intralaminar thalamus, before (blue) and after coactivation. The number of mice used is indicated in parentheses. Data points represent mean ± SEM (*P < 0.05, **P < 0.01, paired t test).

www.manaraa.com

light intensity per unit area. Our estimate of the total number of neurons required for the enhancement was more than ~6,000 (*Materials and Methods*). Photostimulation used in our study evoked neuronal responses across different cortical layers, and the current imaging method could not capture all activated neurons located at various depths and over large areas (millimeters). Previous studies had estimated the number of neurons based on the distribution of light intensity in the brain tissue and the light intensity required for the activation of ChR2-expressing neurons (31). Our estimate was based on fluorescent cells within the area covered by the light with the intensity that reliably triggered neuronal spiking, thus reflecting only the amount of directly activated neurons in the local area.

Neural Circuits Underlying Global Spread of Excitability. The optogenetic stimulation in our experiment primarily activated layer 2/3 cells. The spread of excitability enhancement is likely to be mediated by activation of the layer 5/6 neurons which receive excitatory inputs from layer 2/3 neurons and send long-range projections to other cortical areas and subcortical regions, including the thalamus and striatum (32–36). Our results indicate the midline/intralaminar thalamus was activated during optogenetic stimulation of cortical neurons in V1, but this activation is likely to be indirect because the midline thalamus receives input mainly from the medial prefrontal cortex (37), which was not stimulated in the present study, and the intralaminar thalamus receives mainly indirect projections of cortical neurons through monosynaptic input from mesencephalic reticular formation (38). However, midline/intralaminar thalamic neurons could project diffusely to both the cortex and striatum (38). Thus, the spread of the cortical excitation during coactivation could be mediated through the midline/intralaminar thalamus, as suggested by the results from our chemogenetic suppression experiments.

A surprising finding of this study is that the enhancement effect of coactivation could spread not only within the coactivated cortex but also to the contralateral cortex not coactivated. Cross-hemispheric spread of the enhancement effect could be attributed to direct contralateral neuronal excitation during coactivation (*SI Appendix*, Fig. S6F), via the corpus callosum or subcortical relay. Indeed, activation of the thalamic nucleus in one hemisphere could elicit bilateral excitation in many sensory cortices (20).

A distinct feature of the enhancement effect is the cooperativity among neurons activated in different areas, as indicated by the nonlinear increase of the enhancement effect as the total coactivated area was increased (Figs. 2D and 5D). Interestingly, such cooperativity could occur among neurons distributed over long distances within one hemisphere or even in two hemispheres. The magnitude of the enhancement effect was shown to be distance-independent by experiments in which the distances between coactivated areas were increased progressively (Fig. 5C). These findings support the notion that the global spread of the enhancement effect was mediated by mechanisms that integrate and propagate cortical neuronal excitation in a manner that is insensitive to the location of excited cortical neurons. The thalamus could serve the function of "integrative hub" for the cortical excitation, as previously implicated by brain imaging data (39).

Repetitive Neuronal Coactivation and Global Activity Waves. Besides thalamocortical circuits, corticocortical connections may also contribute to the enhancement effect of global excitability. Spontaneous and sensory-driven waves of neuronal activity across the cortical surface have been observed (13, 40–42). Such waves could coordinate neuronal activities in multiple cortical areas, modify the synaptic efficacy of cortical connections, and play a regulatory role in sensory perception and multisensory integration (43–47). In our experiments, coactivation of the large population of cortical neurons may generate cortical waves that modify neuronal excitability in distant regions. Furthermore, we found that burst stimulation at 30-Hz frequency (gamma band) showed higher efficiency than low-frequency stimulation (5 and 0.05 Hz) for the modification (Fig. 2E), suggesting that gamma-frequency neuronal activation may provide a more effective means for generating cortical waves than low-frequency activation.

Although the primary target of our light stimulation was CaMKII-expressing pyramidal neurons, GABAergic interneurons could also be activated indirectly, and their synchronous coactivation at gamma-range frequency may facilitate gamma oscillations of cortical neurons (48, 49), contributing to the enhancement effect.

Physiological Implications. Noninvasive brain stimulation including transcranial magnetic stimulation (TMS) and transcranial direct-current stimulation (tDCS) are valuable tools for therapeutic modulation of brain activity. Electroencephalography recording and functional brain imaging studies have shown that repetitive application of TMS or tDCS appeared to alter cortical activity both in the stimulated area and in distant brain regions (50, 51). The underlying mechanism for the distant effect of this activation of large populations of cortical neurons is largely unknown. Our finding that repetitive coactivation of large populations of cortical neurons caused a long-term global enhancement effect suggests a potential mechanism underlying the nonlocal effect of repetitive TMS and tDCS, through coactivation of large populations of cortical neurons and global enhancement of cortical excitability.

Repetitive coactivation over large neuronal populations is often associated with pathological conditions such as epilepsy (52). Our results suggest that a seizure triggered at epileptic foci could cause increased excitability of both local and distant circuits, leading to widespread pathological excitability. This may contribute to the understanding of the mechanism underlying progressive epilepsy (53, 54). Furthermore, it is well-known that epilepsy in general and temporal lobe epilepsy in particular is associated with a number of comorbidities. For example, temporal lobe epilepsy is often accompanied by depression, anxiety, dementia, and migraine (55). Seizure-induced global changes in neural circuits shared by many brain functions could be attributed in part to the global enhancement of neuronal excitability due to epileptic discharges.

Materials and Methods

Full descriptions including experimental procedures for animal surgery, viral transfection, multiunit recording, in vivo whole-cell recording, estimation of light intensity for test and coactivation stimuli, drug infusion, data analysis, estimation of the number of neurons activated by optogenetic stimulation, and immunostaining and confocal imaging are described in detail in *SI Appendix, Materials and Methods*. Animal care and experimental procedures were approved by the Animal Care Committee of the Shanghai Institutions for Biological Sciences, Chinese Academy of Sciences.

Data Availability. All study data are included in the article and *SI Appendix*.

Zhang et al.

www.manaraa.com

1. P. Mégevand et al., Long-term plasticity in mouse sensorimotor circuits after rhythmic whisker stimulation. J. Neurosci. 29, 5326–5335 (2009).

2. F. Gambino et al., Sensory-evoked LTP driven by dendritic plateau potentials in vivo. Nature 515, 116–119 (2014).

3. F. Engert, H. W. Tao, L. I. Zhang, M. M. Poo, Moving visual stimuli rapidly induce direction sensitivity of developing tectal neurons. Nature 419, 470–475 (2002).

4. H. Yao, Y. Dan, Stimulus timing-dependent plasticity in cortical processing of orientation. Neuron 32, 315–323 (2001).

5. X. Wang, M. M. Merzenich, K. Sameshima, W. M. Jenkins, Remodelling of hand representation in adult cortex determined by timing of tactile stimulation. Nature 378, 71–75 (1995).

6. W. C. Clapp, I. J. Kirk, J. P. Hamm, D. Shepherd, T. J. Teyler, Induction of LTP in the human auditory cortex by sensory stimulation. Eur. J. Neurosci. 22, 1135–1140 (2005).

7. B. M. Kampa, M. M. Roth, W. Göbel, F. Helmchen, Representation of visual scenes by local neuronal populations in layer 2/3 of mouse visual cortex. Front. Neural Circuits 5, 18 (2011).

8. K. Ohki, S. Chung, Y. H. Ch'ng, P. Kara, R. C. Reid, Functional imaging with cellular resolution reveals precise micro-architecture in visual cortex. Nature 433, 597–603 (2005).

9. J. Sawinski et al., Visually evoked activity in cortical cells imaged in freely moving animals. Proc. Natl. Acad. Sci. U.S.A. 106, 19557–19562 (2009).

10. L. Carrillo-Reid, W. Yang, Y. Bando, D. S. Peterka, R. Yuste, Imprinting and recalling cortical ensembles. Science 353, 691–694 (2016).

11. T. Kim, W. C. Oh, J. H. Choi, H. B. Kwon, Emergence of functional subnetworks in layer 2/3 cortex induced by sequential spikes in vivo. Proc. Natl. Acad. Sci. U.S.A. 113, E1372–E1381 (2016).

12. G. Buzsáki, A. Draguhn, Neuronal oscillations in cortical networks. Science 304, 1926–1929 (2004).

13. H. Zhang, A. J. Watrous, A. Patel, J. Jacobs, Theta and alpha oscillations are traveling waves in the human neocortex. Neuron 98, 1269–1281.e4 (2018).

14. L. Muller, F. Chavane, J. Reynolds, T. J. Sejnowski, Cortical travelling waves: Mechanisms and computational principles. Nat. Rev. Neurosci. 19, 255–268 (2018).

15. C. C. Petersen, A. Grinvald, B. Sakmann, Spatiotemporal dynamics of sensory responses in layer 2/3 of rat barrel cortex measured in vivo by voltage-sensitive dye imaging combined with whole-cell voltage recordings and neuron reconstructions. J. Neurosci. 23, 1298–1309 (2003).

16. A. Stroh et al., Making waves: Initiation and propagation of corticothalamic Ca²⁺ waves in vivo. Neuron 77, 1136–1150 (2013).

17. T. V. Bliss, T. Lomo, Long-lasting potentiation of synaptic transmission in the dentate area of the anaesthetized rabbit following stimulation of the perforant path. J. Physiol. 232, 331–356 (1973).

18. M. F. Bear, R. C. Malenka, Synaptic plasticity: LTP and LTD. Curr. Opin. Neurobiol. 4, 389–399 (1994).

19. R. W. Chan et al., Low-frequency hippocampal-cortical activity drives brain-wide resting-state functional MRI connectivity. Proc. Natl. Acad. Sci. U.S.A. 114, E6972–E6981 (2017).

20. A. T. Leong et al., Long-range projections coordinate distributed brain-wide neural activity with a specific spatiotemporal profile. Proc. Natl. Acad. Sci. U.S.A. 113, E8306–E8315 (2016).

21. J. Liu et al., Frequency-selective control of cortical and subcortical networks by central thalamus. eLife 4, e09215 (2015).

22. M. Deschenes, J. Bourassa, A. Parent, Striatal and cortical projections of single neurons from the central lateral thalamic nucleus in the rat. Neuroscience 72, 679–687 (1996).

23. A. S. Mitchell et al., Advances in understanding mechanisms of thalamic relays in cognition and behavior. J. Neurosci. 34, 15340–15346 (2014).

24. L. A. Newman, J. A. Burk, Effects of excitotoxic thalamic intralaminar nuclei lesions on attention and working memory. Behav. Brain Res. 162, 264–271 (2005).

25. C. Bassetti, J. Mathis, M. Gugger, K. O. Lovblad, C. W. Hess, Hypersomnia following paramedian thalamic stroke: A report of 12 patients. Ann. Neurol. 39, 471–480 (1996).

26. P. Castaigne et al., Paramedian thalamic and midbrain infarct: Clinical and neuropathological study. Ann. Neurol. 10, 127–148 (1981).

27. F. Plum, Coma and related global disturbances of the human conscious state. Cereb. Cortex 9, 359–425 (1991).

28. B. N. Armbruster, X. Li, M. H. Pausch, S. Herlitze, B. L. Roth, Evolving the lock to fit the key to create a family of G protein-coupled receptors potently activated by an inert ligand. Proc. Natl. Acad. Sci. U.S.A. 104, 5163–5168 (2007).

29. W. Zhang, D. J. Linden, The other side of the engram: Experience-driven changes in neuronal intrinsic excitability. Nat. Rev. Neurosci. 4, 885–900 (2003).

30. D. Debanne, M. M. Poo, Spike-timing dependent plasticity beyond synapse—Pre- and post-synaptic plasticity of intrinsic neuronal excitability. Front. Synaptic Neurosci. 2, 21 (2010).

31. D. Huber et al., Sparse optical microstimulation in barrel cortex drives learned behaviour in freely moving mice. Nature 451, 61–64 (2008).

32. M. Levesque, A. Charara, S. Gagnon, A. Parent, M. Deschenes, Corticostriatal projections from layer V cells in rat are collaterals of long-range corticofugal axons. Brain Res. 709, 311–315 (1996).

33. P. Veinante, P. Lavallée, M. Deschênes, Corticothalamic projections from layer 5 of the vibrissal barrel cortex in the rat. J. Comp. Neurol. 424, 197–204 (2000).

34. A. M. Hattox, S. B. Nelson, Layer V neurons in mouse cortex projecting to different targets have distinct physiological properties. J. Neurophysiol. 98, 3330–3340 (2007).

35. R. Aronoff et al., Long-range connectivity of mouse primary somatosensory barrel cortex. Eur. J. Neurosci. 31, 2221–2233 (2010).

36. K. D. Harris, G. M. Shepherd, The neocortical circuit: Themes and variations. Nat. Neurosci. 18, 170–181 (2015).

37. Y. D. Van der Werf, M. P. Witter, H. J. Groenewegen, The intralaminar and midline nuclei of the thalamus. Anatomical and functional evidence for participation in processes of arousal and awareness. Brain Res. Brain Res. Rev. 39, 107–140 (2002).

38. M. Steriade, L. L. Glenn, Neocortical and caudate projections of intralaminar thalamic neurons and their synaptic excitation from midbrain reticular core. J. Neurophysiol. 48, 352–371 (1982).

39. K. Hwang, M. A. Bertolero, W. B. Liu, M. D'Esposito, The human thalamus is an integrative hub for functional brain networks. J. Neurosci. 37, 5594–5607 (2017).

40. I. Ferezou et al., Spatiotemporal dynamics of cortical sensorimotor integration in behaving mice. Neuron 56, 907–923 (2007).

41. J. B. Wekselblatt, E. D. Flister, D. M. Piscopo, C. M. Niell, Large-scale imaging of cortical dynamics during sensory perception and behavior. J. Neurophysiol. 115, 2852–2866 (2016).

42. L. Muller et al., Rotating waves during human sleep spindles organize global patterns of activity that repeat precisely through the night. eLife 5, e17267 (2016).

43. A. J. Borgdorff, J. F. Poulet, C. C. Petersen, Facilitating sensory responses in developing mouse somatosensory barrel cortex. J. Neurophysiol. 97, 2992–3003 (2007).

44. A. A. Ghazanfar, C. E. Schroeder, Is neocortex essentially multisensory? Trends Cogn. Sci. 10, 278–285 (2006).

45. L. A. Ibrahim et al., Cross-modality sharpening of visual cortical processing through layer-1-mediated inhibition and disinhibition. Neuron 89, 1031–1045 (2016).

46. G. A. Calvert et al., Activation of auditory cortex during silent lipreading. Science 276, 593–596 (1997).

47. A. E. Allen, C. A. Procyk, T. M. Brown, R. J. Lucas, Convergence of visual and whisker responses in the primary somatosensory thalamus (ventral posterior medial region) of the mouse. J. Physiol. 595, 865–881 (2017).

48. J. A. Cardin et al., Driving fast-spiking cells induces gamma rhythm and controls sensory responses. Nature 459, 663–667 (2009).

49. V. S. Sohal, F. Zhang, O. Yizhar, K. Deisseroth, Parvalbumin neurons and gamma rhythms enhance cortical circuit performance. Nature 459, 698–702 (2009).

50. H. R. Siebner, U. Ziemann, Rippling the cortex with high-frequency (>100 Hz) alternating current stimulation. J. Physiol. 588, 4851–4852 (2010).

51. S. L. Liew, E. Santarnecchi, E. R. Buch, L. G. Cohen, Non-invasive brain stimulation in neurorehabilitation: Local and distant effects for motor recovery. Front. Hum. Neurosci. 8, 378 (2014).

52. P. Jiruska et al., Synchronization and desynchronization in epilepsy: Controversies and hypotheses. J. Physiol. 591, 787–797 (2013).

53. W. R. Gowers, Epilepsy and Other Chronic Convulsive Disorders, (J & A Churchill, London, 1881).

54. A. C. Coan, F. Cendes, Epilepsy as progressive disorders: What is the evidence that can guide our clinical decisions and how can neuroimaging help? Epilepsy Behav. 26, 313–321 (2013).

55. M. R. Keezer, S. M. Sisodiya, J. W. Sander, Comorbidities of epilepsy: Current concepts and future perspectives. Lancet Neurol. 15, 106–115 (2016).

www.manaraa.com